Welding in the World (2018) 62:267–275
https://doi.org/10.1007/s40194-017-0537-7

RESEARCH PAPER

Wire-based additive manufacturing using an electron beam as heat source

J. Fuchs[1] · C. Schneider[1] · N. Enzinger[1]

Received: 19 September 2017 / Accepted: 4 December 2017 / Published online: 8 January 2018

Abstract
Many standard welding processes, such as gas metal arc-, laser-, or electron-beam welding, can be used for additive manufacturing (AM) with only slight adaptions. Wire-based additive manufacturing provides an interesting alternative to powder-based processes due to their simplicity and comparatively high deposition rates. The use of an electron beam as heat source for AM offers unique possibilities for construction of components due to its inherent flexibility. It is possible to efficiently build bigger parts with comparably fine features and high complexity. Furthermore, additional working steps such as preheating, surface modification, welding, or heat treatments can be implemented into the additive manufacturing process and thereby alleviate the bottleneck of the evacuation of the vacuum chamber. Aside from this, the ultra high vacuum atmosphere can be beneficial, when working with reactive materials such as Ti or Mo. The intrinsic complexity of electron-beam additive manufacturing (EBAM) can make a stable and reproducible process control quite challenging. In this study, the influence of the main process parameters, such as heat input, energy distribution, wire feed, and their complex interactions are investigated. Based on single beads on a mild steel substrate using an unalloyed metal core wire (G4Si1), the correlation between the process parameters such as beam current, acceleration voltage, speed, wire feed rate and position, and the resulting bead geometry, height, width and penetration was studied. These findings were used to successfully establish a multi pass layout consisting of one to six beads next to each other and up to ten layers in height. For basic characterization, metallographic analysis as well as hardness measurements were performed.

Keywords Electron beam · Additive manufacturing · Mild steel · Process development

1 Introduction

Additive manufacturing (AM) is a very promising technology with a huge potential for changing industry fundamentally. Per definition, AM stands for series production using generative processes [1]. Due to the capability to build up parts, layer by layer, directly from 3D data, every part can be optimized to its individual task. Lightweight constructions, complex parts, short time to market and a massive save of resources are just a few advantages of this technology.

Powder-bed processes, such as selective laser melting, selective laser sintering or electron-beam melting, are very common for AM. They provide the possibility for producing very complex parts with tiny features at a good geometric accuracy. For selected materials, parameter sets are given. They are optimized for high deposition rates or for good material properties [2]. Due to the usage of powder in the micrometer range, the achievable deposition rates are limited. Also, the common dimensions of working chambers of machines are limited.

Wire-based additive manufacturing provides an interesting alternative to widen the field of applications. Highly developed welding processes can be used for this task [3]. Many different materials are available, and most of them are even standardized and characterized for standard welding processes. Synergy effects can be used, e.g. in quality control. Main

This article is part of the collection Welding, Additive Manufacturing and Associated NDT

✉ J. Fuchs
juergenfuchs87@gmail.com

C. Schneider
christian.schneider@tugraz.at

N. Enzinger
norbert.enzinger@tugraz.at

[1] Institute of Materials Science, Joining and Forming, Kopernikusgasse 24, 8010 Graz, Austria

Table 1 Chemical composition of G4Si1 in wt%

C	Mn	Si	Fe
0.1	1.0	1.7	Bal.

groups of wire-based additive manufacturing are arc-, laser-, and electron-beam additive manufacturing [4]. The main idea is to economically build up near net shape parts, where just a few subtractive manufacturing steps are needed to achieve the final geometry.

The electron beam is a highly advanced tool, for joining materials as well as for additive manufacturing. The ultra-high vacuum in the working chamber ensures the protection against the negative influence of the atmosphere. This is very beneficial, especially when working with reactive materials. Furthermore, several additional working steps, such as preheating, welding, surface-, or heat treatments can be implemented in the additive manufacturing process.

Establishing the process of EBAM means understanding the fundamental relations between very complex physical processes. A proper attunement of energy input and wire feed is essential for a stable material transfer from the wire to the melt pool and therefore for the formation of a stable melt pool [5]. Controlling melt pool dimensions and melt pool temperature is the key for process control of EBAM [6, 7, 9]Beside energy and material input the conditions for heat transfer influence the formation of the melt pool [10, 11]. During solidification the weld beads are formed. Knowledge of single bead profiles opens the capability for finding an optimum overlapping distance and is an important input for the path planning for more complex geometries [12]. Finally, microstructural evolution and the formation of residual stress leads to the mechanical properties of the work part.

2 Materials and methods

For all experiments, the unalloyed solid wire G4Si1 (EN ISO 14341) was used. The diameter of the wire was 1.2 mm. The chemical composition is listed in Table 1. As substrate, the hot-rolled, high-strength low-alloyed steel S 500 MC was used. The dimensions of the metal sheets were 200 × 125 × 10 mm.

The experiments were performed on the electron-beam welding machine Probeam EBG45-150 K14. The pressure in the working chamber was 5×10^{-4} mbar.

As preparation for light optical microscopy, the samples were ground, polished, and etched with 3% Nital solution.

The dilution was determined according to the following equation

$$dilution = \frac{A_2}{A_1 + A_2}(\%) \quad (1)$$

Thereby A_1 is the part of the bead cross section, which represents the additional filler material, and A_2 is the molten substrate cross section as shown in Fig. 1.

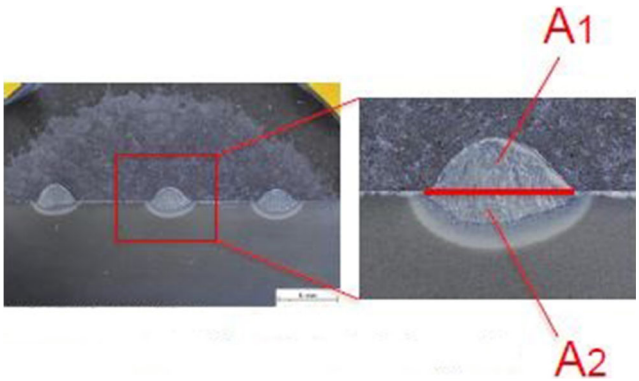

Fig. 1 Measurement of dilution of a single bead

3 Experiments

All welds were performed in the same direction, by welding with the wire directed toward the finished part of the weld. The welding speed was kept constant at 10 mm/s, and the angle between welding direction and wire feed was 35° for all welds (compare Fig. 2).

3.1 Single bead welds

To study the interaction between the main parameters, single beads with a length of 80 mm were welded. The parameters were assigned to the groups of energy input, energy distribution, and wire feed. Follwing aspects were of particular interest:

1. A correct adjustment of the wire feed unit had to be found to ensure a stable and continuous material transfer.
2. Wire feed rate and the energy input had to be attuned for producing optimum results. In this context, also the scheme of beam deflection was optimized.

3.1.1 Adjustment of wire feed

A proper adjustment of the position of the wire feed unit in relation to the work part and the electron beam is compulsory for a stable material transfer. During the welding process, there has to be a liquid bridge of metal between the melting wire and the melt pool [5].

For this study, the auxiliary quantity h, shown in Fig. 2, was introduced. It measures the vertical distance between the top of the work piece and the point of intersection of the wire and the electron beam.

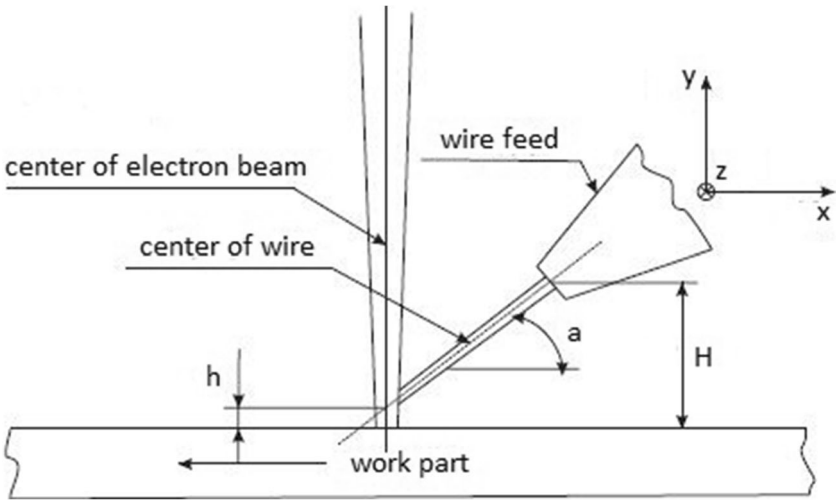

Fig. 2 Adjustment of the wire feed unit in relation to the work piece

Single beads were welded with *h* varying between 0.3 and 3.2 mm. All main parameters are listed in Table 2.

3.1.2 Attunement of wire feed rate and energy input

When reproducible weld beads were achieved, the heat input had to be optimized in order to minimize the dilution and maximize the deposition and growth rate.

For this issue, wire feed rate and beam current were varied on three levels, and the dilution of each bead was measured. The combinations of beam current and wire feed rates are listed in Table 3; all other parameters were set according to Table 2.

3.1.3 Beam deflection

The high energy density of the electron-beam welding process is very beneficial for most applications. In the case of EBAM, where penetration of the beam into the base material is requested to be low and vaporization of metal has to be avoided, energy input has to be limited.

The high frequency oscillation of the electron beam allows for customized energy distribution throughout the work piece. A variety of beam figures differing in size and shape were tested to find the optimum setting for EBAM.

Table 2 Welding parameters for adjustment of wire feed unit

Parameter	Value	Unit
Acceleration voltage	120	kV
Beam current	15	mA
Welding speed	10	mm/s
Wire feed rate	1.5	m/min
Height, *H*	12	mm
Angle, a	35	°

3.1.4 Scalability of main parameters

The possibility to adjust the bead dimensions and deposition rate for individual parts is of great importance for AM. Therefore, the scalability of the main parameters, beam current, and wire feed rate, was investigated.

- The wire feed rate was increased by the factor of 2.5, from 1.8 to 4.5 m/min.
- The beam current was increased by the same factor, from 16 to 40 mA.
- The amplitude of the beam deflection figure was also increased from 3 to 5 mm due to wider expected weld beads.

3.2 Single track multi pass welds

Welding single track multi pass welds was the most critical task in this investigation. The exact positioning of the wire feed in the x-z plane (see Fig. 2) is pivotal for achieving an upright structure (Fig. 8).

Furthermore, adjusting the heat input correctly proved to be crucial. Due to the changed conditions for heat transfer, the heat input has to be decreased with increasing layer number. From the fifth layer onward, the heat input was held constant. Same as in welding single beads, the

Table 3 Combinations of wire feed rate and beam current

	Wire feed rate (m/min)			
Beam current (mA)		1.5	1.8	2.1
	10	×	×	×
	12.5	×	×	×
	15	×	×	×

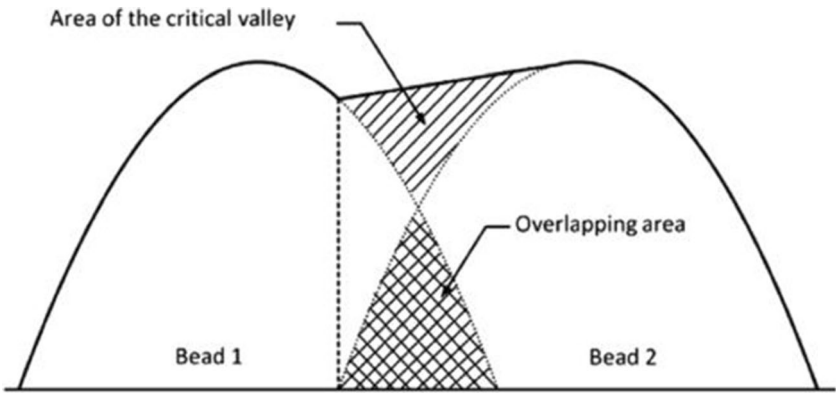

Fig 3 Schematic view of bead overlapping [8]

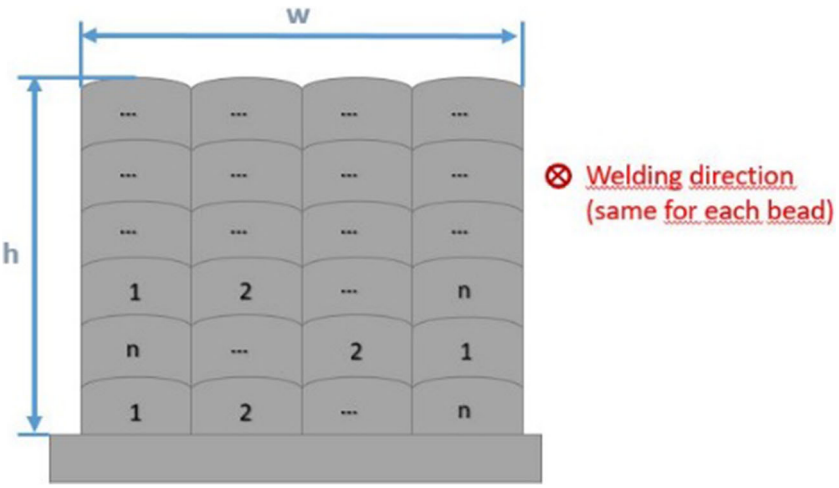

Fig. 4 Weld sequences in multi track welds

welding direction was the same for each layer when building up these structures.

3.3 Multi track multi pass welds

Before welding multi track welds, an optimum overlapping distance between two single beads had to be found. For this study, it was experimentally determined at 80% of single bead width (Fig. 3).

Figure 4 gives an overview of the weld sequence for multi-track multi-pass welds. Welding direction was the same for each bead. The first bead of a layer was set alternating on the left and right side of the structure. The energy input was reduced for bead 1 and for bead *n* of each layer. There was no decrease of heat input with increasing layer number.

4 Results

4.1 Single bead welds

4.1.1 Adjustment of wire feed unit

It was shown that the adjustment of the wire feed unit plays an important role for the process. Figure 5 shows single beads which were made with the same parameter set, only the value of the auxiliary quantity *h* was changed. In the left picture with *h* set below the optimum ($h = 1.3$ mm), the wire has been drifting to the side. The picture in the center shows a bead which was welded with the optimum $h = 1.6$ mm. The choice of a higher *h* ($h = 3.2$ mm) lead to an unstable material transfer (right picture).

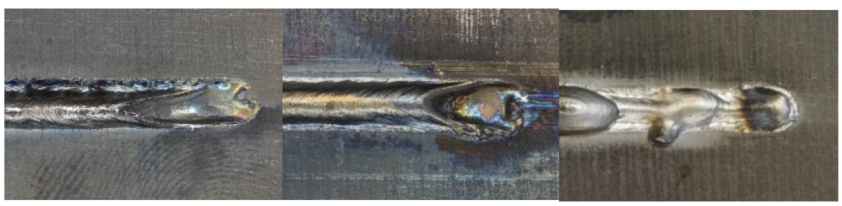

Fig. 5 Adjustment of wire feed, $h <$ optimum (left), $h =$ optimum (center), $h >$ optimum (right)

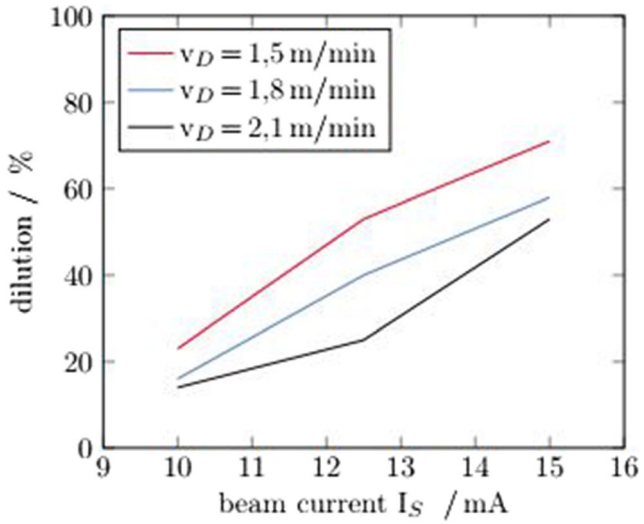

Fig. 6 Dilution dependent on beam current and wire feed rate

4.1.2 Attunement of wire feed rate and heat input

To optimize the heat input and the deposition rate, the dilution in relation to the beam current and wire feed was measured. The results of these measurements are shown in Fig. 6.

It can be seen, that an increase in beam current also leads to an increase in dilution. That can be easily explained by the fact that a higher beam current leads to more heat input and therefore a bigger melt pool, consisting of base and filler metal.

Likewise, a higher wire feed rate results in lower dilution, since the cross section area A_1 (see Eq.(1)) is increased. Furthermore, more energy has to be used to melt the additional filler metal, which decreases the fusion penetration (A_2).

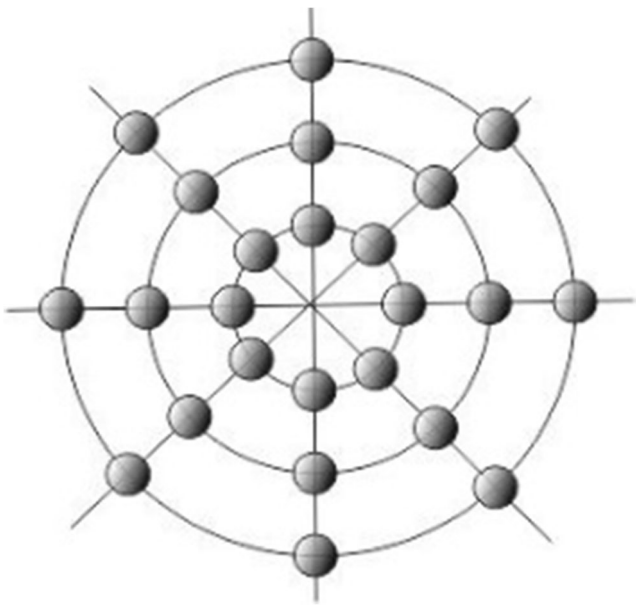

Fig. 7 Beam deflection figure consisting of concentric circles (1000 points)

Table 4 Characteristics of parameter sets A and B

Attribute	set A	set B	unit
Specific energy	143	360	J/mm
Energy per volume	42	42	J/mm^3
Deposition rate	122	305	cm^3/h
Calculated cross section area	3.4	8.5	mm^2
Single bead height	1.4	2.0	mm
Single bead width	2.5	4.5	mm
Optimum h	1.3	2.5	mm

4.1.3 Beam deflection

It was found that the best energy distribution of the electron beam for EBAM can be achieved by a beam figure consisting of concentric circles, Fig. 7. The size of the beam figure is adjusted to the expected weld bead width, in our case 3, resp. 5 mm.

The other tested beam figures, circle, and ellipse, lead to excessive melting of the base metal and therefore higher dilution.

4.1.4 Scalability of main parameters

In order to increase the deposition rate and additionally increase the bead dimensions, a second parameter set with upscaled parameters (set B) was introduced. By increasing the original wire feed rate and the beam current by a factor of 2.5, the deposition rate could also be increased by the same factor, while maintaining the same energy per volume. Consequently, the dimensions of a single bead also changed. The bead height increased from 1.4 to 2.0 mm and the width from 2.5 to 4.5 mm.

Table 4 shows the characteristics of these two parameter sets, which were used for further investigations.

4.2 Single track multi pass welds

To show the specifics of single track multi pass welds, the structure with the lowest wall thickness is given as an example. Figure 8 shows a single-bead- and a thin-walled structure consisting of five layers; parameter set A was used. The wall has a width of 2.8 mm and a height of 5.6 mm.

It was found that the increase of height with increasing layer number was not linear for single track welds. Table 5 gives an overview about the height increase and the reduction of heat input by increasing layer number.

Table 6 lists the height increase and the reduction of the heat input by increasing layer number when working with parameter set B. The structure consisting of eight layers measures a width of 5.0 mm and a height of 12.8 mm.

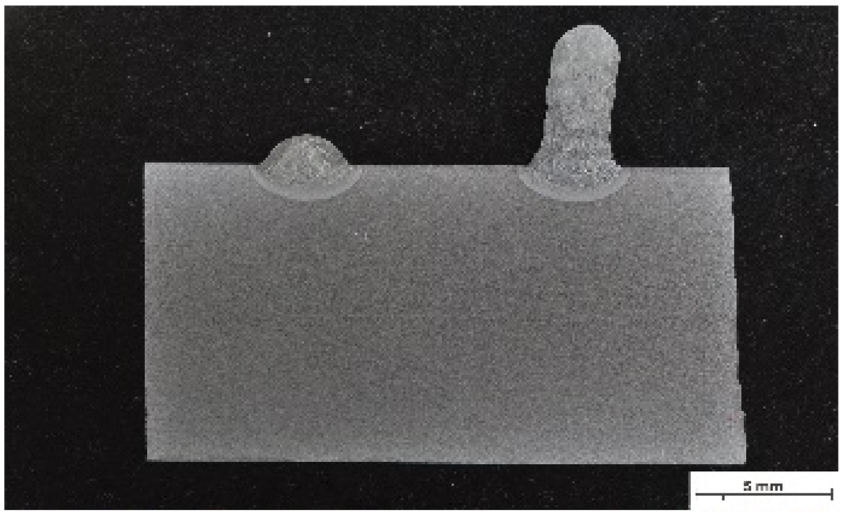

Fig. 8 Single-bead structure consisting of five layers based on set A

Table 5 Height increase and heat input per layer in single-pass welds based on set A

Layer	Height, mm	Specific energy, J/mm	Energy per volume, J/mm^3
1	1.4	144	42
2	1.2	132	39
3	1.0	120	35
4	1.0	108	32
5	1.0	96	28

Table 6 Height increase and heat input per layer in single-pass welds based on set B

Layer	Height, mm	Specific energy, J/mm	Energy per volume, J/mm^3
1	1.8	360	42
2	1.7	338	39
3	1.7	315	35
4	1.6	315	35
5–8	1.5	315	35

4.3 Multi track multi pass welds

The resulting macrostructures of multi pass welds produced with the two different parameter sets A and B were compared using etched cross sections which are shown in Fig. 9. The structure performed with set A (left) consists of seven tracks and nine layers and measures a height of 14 mm and a width of 14 mm. The structure performed with set B (right) consists of three tracks and seven layers and measures a height of 14 mm and a width of 13 mm. The different beads can be easily distinguished in both samples.

4.4 Microstructure

Microstructure was analyzed via light optical microscopy on etched cross sections. Two distinct regions in each sample were compared. The first one is located at the center of a layer, a region which is not influenced by the heat input of a following bead. The second characteristic place is located in the heat affected zone between two single beads.

The microstructure of these characteristic positions is shown in Fig. 10 for set A. In the center of the bead, a

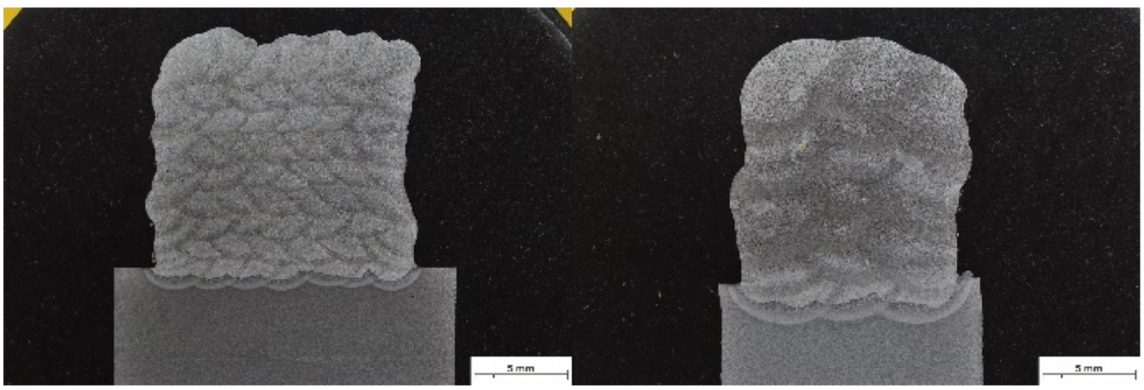

Fig. 9 Structure with seven tracks and nine layers performed with set A (left) and structure with three tracks and seven layers performed with set B (right)

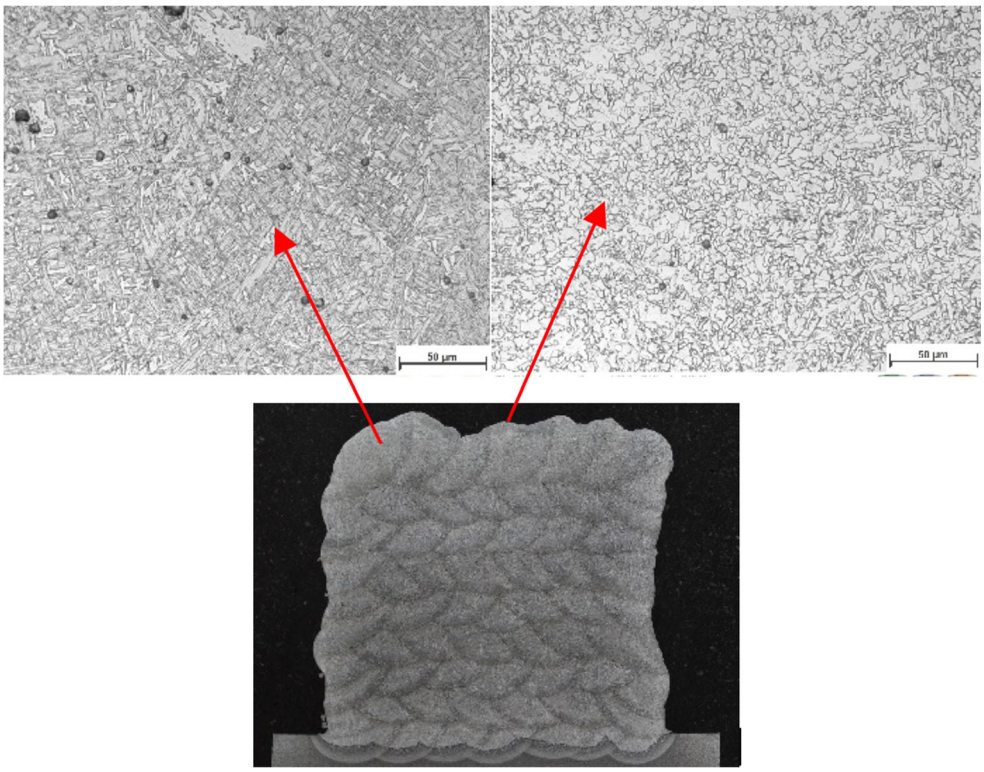

Fig. 10 Microstructure in the center of a bead (upper left) and in the HAZ (upper right), overview (bottom), parameter set A

martensitic microstructure was found (upper left picture). In the heat affected zone, the microstructure consisted mainly of recrystallized globular ferrite (upper right picture). Pores with a size of a few microns have been found all over the cross section.

The microstructure of sample B is shown in Fig. 11. In the center of the bead, Widmannstätten-ferrite was found (upper left picture). In the heat affected zone, the microstructure was again recrystallized globular ferrite (upper right picture). Again, also pores have been found.

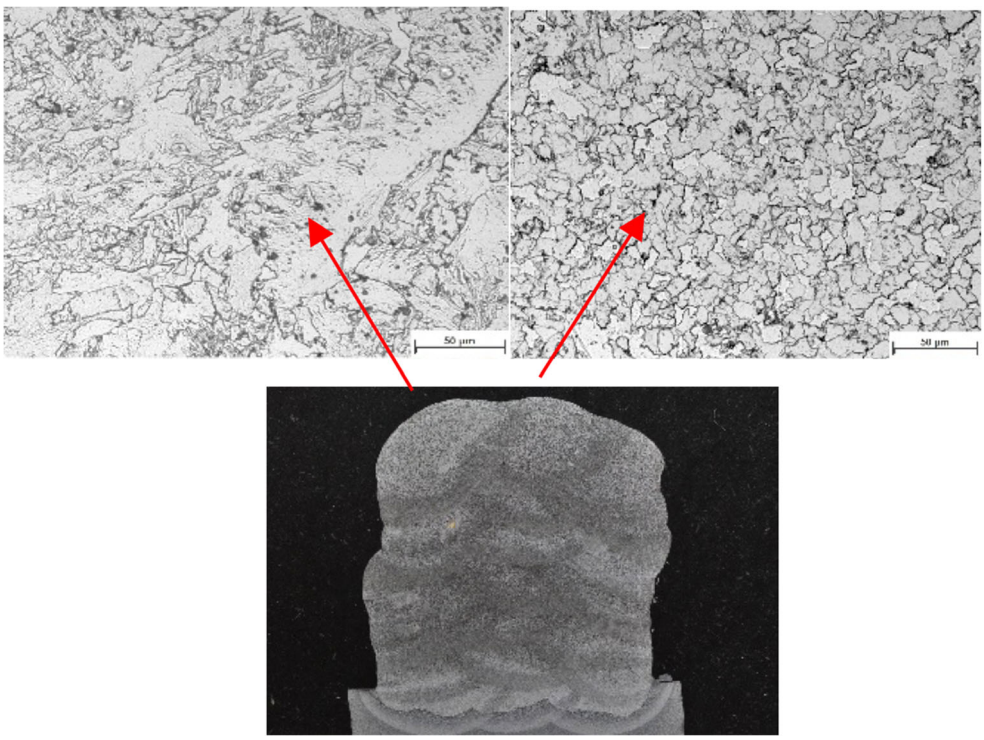

Fig. 11 Microstructure in the centre of a bead (upper left) and in the HAZ (upper right), overview (bottom), parameter set B

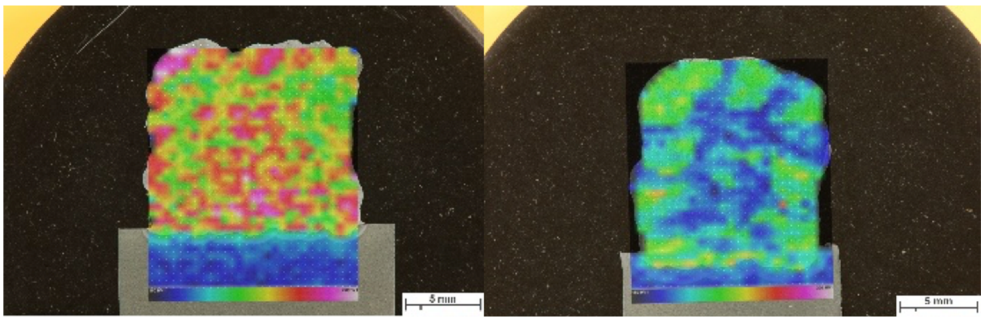

Fig. 12 Hardness map for parameter set A (left) and set B (right), scale from 150 HV1 (blue) to 300 HV1 (white)

The different microstructures from sets A and B, especially in the center of the beads, can be explained by the different heat input and cooling time for different bead sizes. The higher cooling rates in smaller beads, enable the development of martensite, whereas in bigger beads, the critical cooling rate is not reached.

The finer initial microstructure of set A leads also to the finer recrystallized globular microstructure in the heat-affected zone when compared to parameter set B.

4.5 Hardness measurements

Hardness mappings (HV1) have been performed to show local differences in hardness throughout the cross-sections of the two structures. The horizontal and vertical distance between two measurement points was 0.5 mm.

The obtained hardness maps are shown in Fig. 12. For parameter set B, the individual beads can be easily distinguished, whereas for set A, the resolution is not good enough.

The values reach from 188HV1 (green) to 297 HV1 (light pink) for set A. The average measured hardness for this set was 239 HV1. For set B, values ranging from 158 HV1 (dark blue) to 252 HV1 (orange) were measured. The average measured hardness was 194 HV1.

These results are in good agreement with the findings from the microstructure analysis. The finer martensitic microstructure of set A possesses higher hardness than the coarser ferritic microstructure of set B.

5 Conclusion and outlook

5.1 Conclusion

- The process of EBAM was successfully established for unalloyed mild steel.
- In this study, it was found that the position of the wire feed is the key factor to obtain a stable process.
- The deposition rate can be increased by up-scaling the key parameters, beam current, and wire feed rate. Simultaneously the bead dimensions can be influenced by changing the deposition rate.
- Different deposition rates lead to different microstructures due to different cooling rates.

5.2 Outlook

- More complex geometries have to be investigated systematically.
- Temperature measurements, such as melt pool temperature and more important interpass temperature, should be included to ascertain reproducible conditions.
- Different materials, especially reactive metals, such as molybdenum or titanium, should be investigated to make use of the benefit of vacuum-based process.
- Additional working steps, such as heat treatments or surface structure treatments can be implemented.

Acknowledgements Open access funding provided by Graz University of Technology.

Funding information This work was financially supported by Dobeneck-Technologie-Stiftung.

References

1. Fritz, A. H. & Schulze, G., ed. (2015) Fertigungstechnik. Springer Vieweg , Berlin. https://doi.org/10.1007/978-3-662-46555-4
2. EOS, GmbH (2016) Materials for Metal Additive Manufacturing. https://www.eos.info/material-m. Accessed 08 January 2017
3. Stockinger, J., Wiednig, C. A., Enzinger, N., Sommitsch, C., Huber, D., & Stockinger, M. (2016). Additive Manufacturing via Cold Metal Transfer. In Metal Additive Manufacturing Conference: Industrial perspective in Additive Technologies (S. 117-125

4. Ding D, Pan Z, Cuiuri D, Li H (2015) Wire-feed additive manufacturing of metal components: technologies, developments and future interests. Int J Adv Manuf Technol 81(1–4):465–481. https://doi.org/10.1007/s00170-015-7077-3
5. Zhao J, Zhang B, Li X, Li R (2015) Effects of metal-vapor jet force on the physical behavior of melting wire transfer in electron beam additive manufacturing. J Mater Process Tech 220:243–250. https://doi.org/10.1016/j.jmatprotec.2015.01.024
6. Gockel J, Beuth J, Taminger K (2014) Integrated control of solidification microstructure and melt pool dimensions in electron beam wire feed additive manufacturing of Ti-6Al-4V. Addit. Manuf 1–4: 119–126
7. Tang Q, Pang S, Chen B, Suo H, Zhou J (2014) A three dimensional transient model for heat transfer and fluid flow of weld pool during electron beam freeform fabrication of Ti-6-al-4-V alloy. Int J Heat Mass Transf 78:203–215. https://doi.org/10.1016/j.ijheatmasstransfer.2014.06.048
8 Ding D, Pan Z, Cuiuri D, Li H (2015) A multi-bead overlapping model for robotic wire and arc additive manufacturing. Robot Comput Integr Manuf 31:101–110. https://doi.org/10.1016/j.rcim.2014.08.008
9 Gockel J, Fox J, Beuth J, Hafley R (2015) Integrated melt pool and microstructure control for Ti–6Al–4V thin wall additive manufacturing. Mater Sci Technol 31(8):912–916. https://doi.org/10.1179/1743284714Y.0000000704
10 Thompson SM, Bian L, Shamsaei N, Yadollahi A (2015) An overview of direct laser deposition for additive manufacturing Part I: transport phenomena, modeling and diagnostics. Addit Manuf 8: 36–62. https://doi.org/10.1016/j.addma.2015.07.001
11 Jandric Z, Kovacevic R (2004) Heat management in solid free-form fabrication based on deposition by welding. Proc Inst Mech Eng Part B: J Eng Manuf 218(11):1525–1540. https://doi.org/10.1243/0954405042418545
12 Ding D, Pan Z, Cuiuri D, Li H, Van Duin S, Larkin N (2016) Bead modelling and implementation of adaptive MAT path in wire and arc additive manufacturing. Robot Comput Integr Manuf 39:32–42. https://doi.org/10.1016/j.rcim.2015.12.004